RSC Advances

PAPER

View Article Online
View Journal | View Issue

Cite this: *RSC Adv.*, 2021, **11**, 7271

A Brønsted acidic ionic liquid anchored to magnetite nanoparticles as a novel recoverable heterogeneous catalyst for the Biginelli reaction†

Hourieh Sadat Oboudatian, Hossein Naeimi and Mohsen Moradian *

Received 23rd November 2020
Accepted 27th January 2021

DOI: 10.1039/d0ra09929e

rsc.li/rsc-advances

In this study, simple and effective methods were used for the preparation of an ionic liquid that immobilized magnetite nanoparticles. Fe_3O_4 nanoparticles were prepared *via* a chemical co-precipitation method. Then, a SiO_2 shell was coated on the magnetic core *via* the Stober method. Finally, CPTES (chloropropyltriethoxysilane) and morpholine were coated on the SiO_2 shell. Morpholine sulfate, an acidic ionic liquid, was successfully bound to magnetite nanoparticles (Mag@Morph-AIL) and this was used as an efficient catalyst for the preparation of 3,4-dihydropyrimidinones. Compared to previous works, the easy separation of the nanocatalyst using an external magnet and the recyclability, non-toxicity, versatility, and high stability of the catalyst, combined with low reaction times and excellent yields, make the present protocol very useful for the synthesis of the title products. The synthesized products and catalyst were confirmed *via* ^{1}H-NMR, ^{13}C-NMR, FT-IR, scanning electron microscope, X-ray diffraction, and elemental analysis.

Introduction

Dihydropyrimidinone and its derivatives have attracted significant attention because of their potential activities as calcium channel modulators, antihypertensive agents, and antagonists agents for neuropeptide Y (NPY) and α-1a-adrenergic receptors.[1–3] Moreover, these compounds are bio-isosteres of dihydropyridines, which have attracted widespread attention because of their vital pharmaceutical and therapeutic properties, for example, anticancer,[4] antifungal,[5] anti-inflammatory,[6] antibacterial,[7] antiviral,[8] antidiabetic,[9] antithyroid,[10] anti-muscarinic,[11] and hypolipidemic activities.[8] Besides, various alkaloids including the dihydropyrimidine moiety have been isolated from natural and marine sources, and they also display interesting biological properties. Hence, the synthesis of a variety of these molecules is desirable and of much current importance.[12]

The synthesis of 3,4-dihydropyrimidinone compounds can be performed under different conditions, including under strongly acidic conditions in a protic solvent.[13–16] It has traditionally been catalysed using strong Brønsted acids; Lewis acids;[17–21] homogeneous acid catalysts, such as polyphosphate esters,[22] $ZnCl_2$, or $CuCl_2$;[23] heterogeneous acid catalysts, like Al-MCM-41 or $FeCl_3$ embedded in Al-MCM-41;[24] nanocomposites;[25,26] nanoparticles;[27] magnetic nanoparticles;[28] metal oxides; and enzymes. Also, this reaction can be modified using microwave irradiation,[29,30] ultrasound irradiation,[31] ionic liquids,[32–34] and organocatalysis,[35] or using a combination of these.

However, despite their potential utility, many of these reported one-pot protocols suffer from shortcomings, such as the use of expensive reagents, long reaction times, low yields, and volatile strongly acidic conditions. Therefore, the introduction of milder and more efficient methods with higher yields is needed. We have investigated the synthesis of 3,4-dihydropyrimidinone derivatives utilizing Fe_3O_4@SiO_2 nanoparticles as recyclable catalysts and eco-friendly materials, based on the principles of green chemistry and with the aim of developing an ideal synthesis approach. Magnetic iron oxide nanoparticles have attracted much research interest in recent years because of their unique physicochemical properties and great potential for various biomedical applications.

The reactivity of catalytic nanoparticles is largely determined by the energy of surface atoms, which can be easily gauged based on the number of neighboring atoms, the bonding modes, and the accompanying energies of the small molecules to be transformed on the surfaces of nanoparticles.[36,37] Applications of magnetic nanoparticles (MNPs) in different industrial and biological fields, such as in magnetic resonance imaging, drug delivery, bioseparation, hyperthermia treatment, and catalytic processes, have been demonstrated.[36–39] Among the various magnetic nanoparticles under investigation, Fe_3O_4 nanoparticles (Fe_3O_4 NPs) are arguably the most extensively studied NPs.

The main characteristics of these nanoparticles are their simplicity and their easy separation from reaction media using

Department of Organic Chemistry, Faculty of Chemistry, University of Kashan, Kashan, 87317, I. R. Iran. E-mail: m.moradian@kashanu.ac.ir; Fax: +98-03155912397; Tel: +98-03155913055

† Electronic supplementary information (ESI) available: FT-IR and H-NMR spectroscopy data. See DOI: 10.1039/d0ra09929e

a magnetic field. Furthermore, the surfaces of magnetic metal oxide NPs, such as magnetic Fe_3O_4 nanoparticles, can be functionalized and modified with various organic and inorganic materials.[40,41] In this study, a morpholine sulfate acidic ionic liquid was bonded to magnetite nanoparticles (Mag@Morph-AIL) as an efficient catalyst, and it was used for the preparation of 3,4-dihydropyrimidinones. Also, we managed to synthesize two new derivatives of 3,4-dihydropyrimidinones (**4k** and **4o**).

Experimental

Materials and method

The chemicals used in this work were purchased from Fluka and Merck Chemical Companies and were used without purification. Infrared (IR) spectra were obtained in KBr pellet form using a PerkinElmer 781 spectrophotometer and an Impact 400 Nicolet FT-IR spectrophotometer. Proton and carbon nuclear magnetic resonance (^{1}H-NMR and ^{13}C-NMR) spectra were recorded in $CDCl_3$ or DMSO solvent using a Bruker DRX-400 spectrometer with tetramethylsilane as an internal reference. The X-ray diffraction analysis (XRD) patterns of samples were obtained using a Philips Xpert X-ray powder diffractometer (CuK radiation, λ = 0.154056 nm). Energy-dispersive X-ray spectroscopy (EDX) spectra of the nanoparticles were obtained using a Sigma ZEISS, Oxford Instruments field-emission scanning electron microscope. The melting points of products were determined using Electrothermal 9200 apparatus and values were uncorrected. Determination of the purity of substrates and reaction monitoring was accomplished *via* thin-layer chromatography (TLC) on silica gel Polygram SILG/UV 254 plates (from Merck Company). Thermogravimetric and differential thermal analysis (TGA-DTA) data were obtained using a Bahr STA-503 instrument in air at a heating rate of 10 °C min^{-1}. Transmission electron microscopy (TEM) images were recorded using a Zeiss-EM10C microscope with an acceleration voltage of 100 kV.

General procedure for the synthesis of the functionalized magnetic nanocatalyst

Synthesis of Fe_3O_4 nanoparticles. Fe_3O_4 nanoparticles were synthesized *via* a chemical co-precipitation method. An aqueous solution of $FeCl_3$ and $FeCl_2$ with an Fe^{2+}/Fe^{3+} molar ratio of 1/2 was prepared and kept at room temperature. For this purpose, 4.05 g of $FeCl_3 \cdot 6H_2O$ and 1.5 g of $FeCl_2 \cdot 4H_2O$ were dissolved in 100 mL of deionized water with the help of an ultrasonic probe. Then, 30 mL of 25% NH_4OH was added into the solution under nitrogen gas under vigorous stirring. The reaction was stirred and refluxed for 1 h at 90 °C under reflux. After adding NH_4OH to the solution, the colour of the solution turned black. The magnetite precipitate was isolated *via* magnetic decantation, which included washing several times with deionized water and ethanol, and then drying at 80 °C for 10 h in an oven.[42,43]

Preparation of Fe_3O_4@SiO_2. The Stober method was used for the preparation of the shell structure (Fe_3O_4@SiO_2). 1 g of magnetite nanoparticles was dispersed in a solution of 10 mL of deionized water and 50 mL of dry ethanol before being sonicated for 10 min. After that, 40 mL of NH_4OH was added to the reaction mixture and it was sonicated again for 10 min. Then, 3 mL of tetraethyl orthosilicate (TEOS) dissolved in 25 mL of ethanol was added dropwise to the solution at room temperature. Then, the reaction was allowed to proceed under continuous magnetic stirring for 18 h. The final product was separated from solution, washed several times with deionized water and ethanol, and then dried at room temperature for 8 h.[44]

Preparation of Fe_3O_4@SiO_2/TES-Cl. Fe_3O_4@SiO_2 (1 g) was dispersed in 50 mL of toluene and sonicated for 60 min. Then 3-chloropropyl-triethoxysilan (10 mmol) was added dropwise to the reaction mixture and it was sonicated for 30 min. The resultant mixture was subsequently refluxed at 140 °C under vigorous stirring for 24 h. The obtained bright brown nanoparticles were magnetically separated, consecutively washed twice with toluene and twice with ethanol, and then dried at 60 °C in an oven.[45]

Preparation of Fe_3O_4@SiO_2/TES-morpholine. 1 g of Fe_3O_4@SiO_2–Cl in 50 mL of CH_3CN was sonicated for 30 min. Then, a solution containing 1.3 mL of morpholine (15 mmol) and 0.1 mL of triethylamine was added dropwise to the reaction mixture, which was then refluxed for 24 h. The solid product was separated from the solution using a bar magnet, washed with deionized water/ethanol, and finally dried at 60 °C in an oven.[46]

Preparation of Mag@Morph-AIL. To create a dispersion, 1 g of the prepared magnetite Fe_3O_4@SiO_2/TES-morpholine nanoparticles was sonicated in 50 mL of dry ethanol for 15 min. Then, sulfuric acid (0.65 mL, 12 mmol) was added dropwise to the reaction mixture and it was refluxed for 4 h. The obtained powder was successfully separated using a bar magnet and washed with ethanol (3 × 30 mL) to remove the remaining acid, before being dried overnight at room temperature.

General procedure for the synthesis of 3,4-dihydropyrimidinones

Ethyl acetoacetate (1 mmol), aromatic aldehyde (1 mmol), urea (1.5 mmol) and 0.06 g of Mag@Morph-AIL as catalyst were added to 30 mL of absolute ethanol in a 50 mL round-bottomed flask, and the mixture was mechanically stirred at 80 °C for an appropriate amount of time. After the completion of the reaction as monitored *via* TLC, 10 mL of ethanol was added to the reaction mixture and stirring was continued at ambient temperature for 10 min. The catalyst was easily isolated using a bar magnet, and the product was obtained after the removal of the solvent under reduced pressure. Then, the product was treated with water followed by crystallization from EtOH. The products were characterized based on ^{1}H-NMR, FT-IR, and melting point analysis, and the spectral data of the synthesized compounds were compared with authentic samples. The data is given below.

Ethyl 6-methyl-2-oxo-4-phenyl-1,2,3,4-tetrahydropyrimidine-5-carboxylate (4a). White solid; mp = 205–209 °C; IR (KBr) ν (cm^{-1}): 3245 (NH), 3119 (NH), 2978 (C–H), 1702 (C=O), 1647, 1464 (C=C), 1223, 1092 (C–O); ^{1}H-NMR ($CDCl_3$, 400 MHz)

δ (ppm): 1.18 (t, J = 14 Hz, 3H, CH_3), 2.36 (s, 3H, CH_3), 4.07 (q, 2H, CH_2), 5.40 (s, 1H, CH), 5.64 (s, 1H, NH), 7.28–7.33 (m, 5H), 7.72 (s, 1H, NH).

Ethyl 4-(2-chlorophenyl)-6-methyl-2-oxo-1,2,3,4-tetrahydropyrimidine-5-carboxylate (4b). White solid; mp = 242–245 °C; IR (KBr) ν (cm^{-1}): 3234 (NH), 3099 (NH), 2934 (C–H), 1704 (C=O), 1643, 1444 (C=C_{arom}), 1221, 1080 (C–O); ^{1}H-NMR (DMSO-d6, 400 MHz) δ (ppm): 0.97 (t, J = 14 Hz, 3H, CH_3), 2.28 (s, 3H, CH_3), 3.88 (q, 2H, CH_2O), 5.61 (s, 1H, CH), 7.21–7.37 (m, 3H), 7.39 (d, J = 6.8 Hz, 1H), 7.71 (s, 1H, NH), 9.26 (s, 1H, NH).

Ethyl 4-(4-chlorophenyl)-6-methyl-2-oxo-1,2,3,4-tetrahydropyrimidine-5-carboxylate (4c). White solid; mp = 210–212 °C; IR (KBr) ν (cm^{-1}): 3243 (NH), 3118 (NH), 2926 (C–H), 1705 (C=O), 1647, 1461 (C=C), 1222, 1089 (C–O); ^{1}H-NMR (DMSO-d6, 400 MHz) δ (ppm): 1.07 (t, J = 12.4 Hz, 3H, CH_3), 2.23 (s, 3H, CH_3), 3.95 (q, 2H, CH_2O), 5.12 (s, 1H, CH), 7.23 (d, J = 7.2 Hz, 2H), 7.38 (d, J = 6 Hz, 2H), 7.77 (s, 1H, NH), 9.25 (s, 1H, NH).

Ethyl 4-(3-hydroxyphenyl)-6-methyl-2-oxo-1,2,3,4-tetrahydropyrimidine-5-carboxylate (4d). Milky solid; mp = 159–163 °C; IR (KBr) ν (cm^{-1}): 3517 (OH), 3243 (NH), 3199 (NH), 2978 (C–H), 1723 (C=O), 1639, 1455 (C=C), 1222, 1092 (C–O); ^{1}H-NMR (DMSO-d6, 400 MHz) δ (ppm): 1.10 (t, J = 14 Hz, 3H, CH_3), 2.22 (s, 3H, CH_3), 3.98 (q, 2H, CH_2O), 5.08 (s, 1H, CH), 6.58–6.70 (m, 3H), 7.08 (dd, J = 15.2 Hz, 1H), 7.68 (s, 1H, NH), 9.15 (s, 1H, NH), 9.36 (1H, OH).

Ethyl 4-(2,4-dichlorophenyl)-6-methyl-2-oxo-1,2,3,4-tetrahydro-pyrimidine-5-carboxylate (4e). White solid; mp = 249–250 °C; IR (KBr) ν (cm^{-1}): 3219 (NH), 3106 (NH), 2970 (C–H), 1699 (C=O), 1643 (C=C), 1456 (C=C), 1225, 1096 (C–O); ^{1}H-NMR ($CDCl_3$, 400 MHz) δ (ppm): 1.00 (t, J = 12 Hz, 3H, CH_3), 2.27 (s, 3H, CH_3), 3.90 (q, 2H, CH_2O), 5.58 (s, 1H, CH), 7.41 (d, J = 8 Hz, 1H), 7.31 (d, J = 6 Hz, 1H), 7.55 (s, 1H, NH), 7.75 (s, 1H), 9.31 (s, 1H, NH).

Ethyl 4-(2-bromophenyl)-6-methyl-2-oxo-1,2,3,4-tetrahydropyrimidine-5-carboxylate (4f). Yellow solid; mp = 180–190 °C; IR (KBr) ν (cm^{-1}): 3226 (NH), 3112 (NH), 2976 (C–H), 1695 (C=O), 1639, 1450 (C=C), 1227, 1096 (C–O); ^{1}H-NMR (DMSO-d6, 400 MHz) δ (ppm): 1.06 (t, J = 12 Hz, 3H, CH_3), 2.44 (s, 3H, CH_3), 4.01 (q, 2H, CH_2O), 5.85 (s, 1H, CH), 7.16 (dd, J = 14.8 Hz, 1H), 7.23–7.28 (m, 2H), 7.27 (s, 1H, NH), 7.55 (d, J = 8 Hz, 1H), 8.82 (s, 1H, NH).

Ethyl 4-(2-fluorophenyl)-6-methyl-2-oxo-1,2,3,4-tetrahydropyrimidine-5-carboxylate (4g). Yellow solid; mp = 222–228 °C; IR (KBr) ν (cm^{-1}): 3229 (NH), 3113 (NH), 2975 (C–H), 1692 (C=O), 1642, 1459 (C=C), 1228, 1100 (C–O); ^{1}H-NMR (DMSO-d6, 400 MHz) δ (ppm): 1.12 (t, J = 12 Hz, 3H, CH_3), 2.41 (s, 3H, CH_3), 4.04 (q, 2H, CH_2O), 5.65 (s, 1H, CH), 5.7 (d, J = 14.4 Hz, 1H), 7.03 (d, J = 8 Hz, 1H), 7.08 (dd, J = 12 Hz, 1H), 7.14 (s, 1H, NH), 7.23 (dd, J = 16 Hz, 1H), 8.16 (s, 1H, NH).

Ethyl 4-(3-nitrophenyl)-6-methyl-2-oxo-1,2,3-tetrahydropyrimidine-5-carboxylate (4h). White solid; mp = 125–128 °C; IR (KBr) ν (cm^{-1}): 3217 (NH), 3101 (NH), 2964 (C–H), 1707 (C=O), 1628, 1455 (C=C), 1526, 1374 (N–O), 1223, 1088 (C–O); ^{1}H-NMR (DMSO-d6, 400 MHz) δ (ppm): 1.08 (t, J = 13.6 Hz, 3H, CH_3), 2.25 (s, 3H, CH_3), 3.99 (q, 2H, CH_2O), 5.28 (s, 1H, CH), 7.63 (d, J = 7.6 Hz, 1H), 7.68 (dd, J = 20 Hz, 1H), 7.91 (s, 1H, NH), 8.07 (s, 1H), 8.13 (d, J = 7.6 Hz, 1H), 9.38 (s, 1H, NH).

Ethyl 4-(4-nitrophenyl)-6-methyl-2-oxo-1,2,3,4-tetrahydropyrimidine-5-carboxylate (4i). White solid; mp = 197–205 °C; IR (KBr) ν (cm^{-1}): 3240 (NH), 3122 (NH), 2985 (C–H), 1703 (C=O), 1644, 1463 (C=C), 1521, 1394 (N–O), 1217, 1092 (C–O); ^{1}H-NMR (DMSO-d6, 400 MHz) δ (ppm): 1.09 (t, J = 13.2 Hz, 3H, CH_3), 2.25 (s, 3H, CH_3), 3.97 (q, 2H, CH_2O), 5.26 (s, 1H, CH), 7.49 (d, J = 7.2 Hz, 2H), 7.89 (s, 1H, NH), 8.21 (d, J = 7.2 Hz, 2H), 9.36 (s, 1H, NH).

Ethyl 4-(anthracen-9-yl)-6-methyl-2-oxo-1,2,3,4-tetrahydropyrimidine-5-carboxylate (4j). Green solid; mp = 280–285 °C; IR (KBr) ν (cm^{-1}): 3226 (NH), 3111 (NH), 2972 (C–H), 1693 (C=O), 1635, 1451 (C=C), 1230, 1099 (C–O); ^{1}H-NMR (DMSO-d6, 400 MHz) δ (ppm): 0.17 (t, J = 14 Hz, 3H, CH_3), 2.22 (s, 3H, CH_3), 3.34 (q, 2H, CH_2O), 3.39 (s, 1H, CH), 7.00 (d, J = 10 Hz, 1H), 7.49 (t, J = 20 Hz, 4H), 7.69 (s, 1H, NH), 8.07 (d, J = 8 Hz, 2H), 8.41 (s, 1H), 8.55 (d, J = 13.6 Hz, 1H), 9.26 (s, 1H, NH).

Ethyl 4-(9,10-dioxo-9,10-dihydroanthracen-2-yl)-6-methyl-2-oxo-1,2,3,4-tetrahydro-pyrimidine-5-carboxylate (4k). Yellow solid; mp = 269–275 °C; IR (KBr) ν (cm^{-1}): 3358 (NH), 3120 (NH), 2974 (C–H), 1702 (C=O), 1673 (C=O), 1639, 1447 (C=C), 1223, 1087 (C–O); ^{1}H-NMR (DMSO-d6, 400 MHz) δ (ppm): 1.00 (t, J = 8 Hz, 3H, CH_3), 2.30 (s, 3H, CH_3), 3.90 (q, 2H, CH_2O), 5.60 (s, 1H, CH), 7.64 (s, 1H, NH), 7.67 (d, J = 8 Hz, 1H), 7.87 (s, 1H), 7.92 (d, J = 8 Hz, 1H), 7.99 (d, J = 8 Hz, 2H), 8.15 (dd, J = 24 Hz, 2H), 9.30 (s, 1H, NH).

Ethyl 4-(4-methylphenyl)-6-methyl-2-oxo-1,2,3,4-tetrahydropyrimidine-5-carboxylate (4l). Yellow solid; mp = 201–204 °C; IR (KBr) ν (cm^{-1}): 3244 (NH), 3115 (NH), 2979 (C–H), 1705 (C=O), 1647, 1460 (C=C), 1222, 1089 (C–O), ^{1}H-NMR (DMSO-d6, 400 MHz) δ (ppm): 1.11 (t, J = 8 Hz, 3H, CH_3), 2.22 (s, 3H, CH_3), 2.24 (s, 3H, CH_3), 3.95 (q, 2H, CH_2O), 5.09 (s, 1H, CH), 7.06 (d, J = 9.6 Hz, 2H), 7.10 (d, J = 9.6 Hz, 2H), 7.66 (s, 1H, NH), 9.15 (s, 1H, NH).

Ethyl 4-(3,4-dimethoxylphenyl)-6-methyl-2-oxo-1,2,3,4-tetrahydro-pyrimidine-5-carboxylate (4m). Milky solid; mp = 178–178.5 °C; IR (KBr) ν (cm^{-1}): 3248 (NH), 3119 (NH), 2934 (C–H), 1706 (C=O), 1652, 1459 (C=C), 1232, 1092 (C–O); ^{1}H-NMR ($CDCl_3$, 400 MHz) δ (ppm): 1.20 (t, J = 14 Hz, 3H, CH_3), 2.35 (s, 3H, CH_3), 3.84 (s, 3H, CH_3), 3.87 (s, 3H, CH_3), 4.10 (q, 2H, CH_2O), 5.61 (s, 1H, CH), 5.66 (s, 1H), 6.75 (s, 1H, NH), 6.80 (d, J = 6.4 Hz, 1H), 6.85 (d, J = 8.4 Hz, 1H), 7.89 (s, 1H, NH).

Ethyl 4-(4-dimethylaminophenyl)-6-methyl-2-oxo-1,2,3,4-tetrahydro-pyrimidine-5-carboxylate (4n). Yellow solid; mp = 257–259 °C; IR (KBr) ν (cm^{-1}): 3242 (NH), 3113 (NH), 2930 (C–H), 1702 (C=O), 1646, 1453 (C=C), 1225, 1090 (C–O); ^{1}H-NMR (DMSO-d6, 400 MHz) δ (ppm): 1.09 (t, J = 12 Hz, 3H, CH_3), 2.21 (s, 3H, CH_3), 2.83 (s, 6H, CH_3), 3.94 (q, 2H, CH_2O), 5.01 (s, 1H, CH), 6.64 (d, J = 8.4 Hz, 2H), 7.03 (d, J = 8.4 Hz, 2H), 7.57 (s, 1H, NH), 9.26 (s, 1H, NH).

Ethyl 4-(isopentyl)-6-methyl-2-oxo-1,2,3,4-tetrahydropyrimidine-5-carboxylate (4o). Orange color solid; mp = 168–170 °C; IR (KBr) ν (cm^{-1}): 3240 (NH), 3112 (NH), 2954 (C–H), 1706 (C=O), 1651, 1466 (C=C), 1219, 1085 (C–O); ^{1}H-NMR (DMSO-d6, 400 MHz) δ (ppm): 0.84 (d, J = 6 Hz, 6H, CH_3), 1.10 (q, 2H, CH_2), 1.18 (t, J = 14 Hz, 3H, CH_3), 1.35 (q, 2H, CH_2), 1.69 (m, 1H, CH), 2.14 (s, 3H, CH_3), 3.32 (q, 2H, CH_2O), 4.04 (t, J = 12.8 Hz, 1H, CH), 7.43 (s, 1H, NH), 8.95 (s, 1H, NH).

Results and discussion

Structural analysis of the Mag@Morph-AIL nanocatalyst

In this work, green and effective methods were used to produce Fe_3O_4@SiO_2/TES-Mo$^+$$HSO_4^-$ nanoparticles. Fe_3O_4 nanoparticles were prepared *via* a chemical co-precipitation method. Then, a SiO_2 shell was coated on the magnetite core *via* the Stober method. Finally, CPTES (chloropropyltriethoxysilane) and morpholine were coated on the SiO_2 shell. The Mag@Morph-AIL nanoparticles were an efficient catalyst that were used for the preparation of 3,4-dihydropyrimidinones (Scheme 1).

FT-IR spectra of Fe_3O_4, Fe_3O_4@SiO_2, and Mag@Morph-AIL are shown in Fig. 1. In the FT-IR spectrum of Fe_3O_4, the peaks at 3410 and 1625 cm^{-1} correspond to O–H stretching and bending vibrations, respectively, and the peak at 583 cm^{-1} corresponds to Fe–O stretching vibrations. In the FT-IR spectrum of Fe_3O_4@SiO_2 (Fig. 1b), the peak at 1092 cm^{-1} corresponds to Si–O stretching vibrations.

In the FT-IR spectrum of Mag@Morph-AIL (Fig. 1c), the S=O stretching vibrations of the –HSO_4 group appeared at 1100–1250 cm^{-1} with a high relative intensity. The peaks at 1467 and 1634 cm^{-1} correspond to N–H and O–H bending vibrations, respectively, and the peak at 3425 cm^{-1} corresponds to N–H and O–H stretching vibrations.

As shown in Fig. 2, the XRD patterns of Fe_3O_4, Fe_3O_4@SiO_2, and Mag@Morph-AIL nanoparticles are provided. The patterns agree well with the reported pattern for Fe_3O_4 nanoparticles. The XRD pattern of Mag@Morph-AIL includes peaks from Fe_3O_4 and the silica layer. According to the Scherrer equation utilizing the FWHM, the average crystalline size of the Mag@Morph-AIL nanoparticles that were obtained was calculated to be 10–15 nm.

As shown in Fig. 3, the hysteresis loops of the samples are completely reversible, confirming their superparamagnetic nature. The catalyst shows high magnetic permeability and high hysteresis loop reversibility. The decrease in the level of catalyst magnetism relative to the initial state indicates the presence of organic groups on the primary surface.

As indicated in Fig. 3, the levels of saturation magnetization for Fe_3O_4@SiO_2 and Mag@Morph-AIL are 50.86 emu g^{-1} and 13.84 emu g^{-1}, respectively. These results determine that the magnetization properties decrease upon coating and functionalization. According to these results, the catalyst can be easily separated and recovered using an external magnetic field.

As shown in Fig. 4, scanning electron microscopy (SEM) imaging indicates that the prepared Mag@Morph-AIL NPs possess an average diameter of about 65 nm, and the nanoparticles show good dispersity with spherical morphology. A TEM image of the Mag@Morph-AIL nanoparticles is shown in Fig. 4d. Here, the TEM image gives more accurate information about the particle size and morphology of the nanomaterial. The TEM image reveals the spherical shape of the

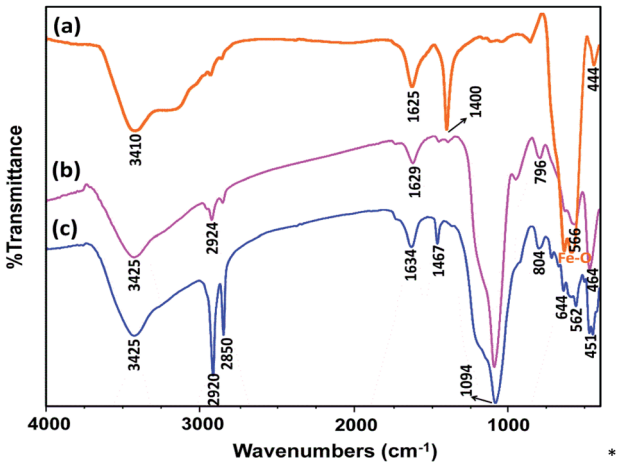

Fig. 1 FT-IR spectra of (a) Fe_3O_4, (b) Fe_3O_4@SiO_2, and (c) Mag@Morph-AIL.

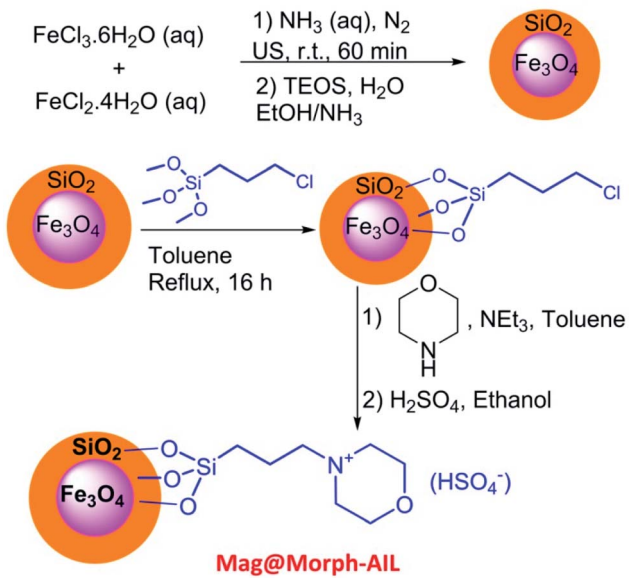

Scheme 1 The preparation of the catalyst Mag@Morph-AIL.

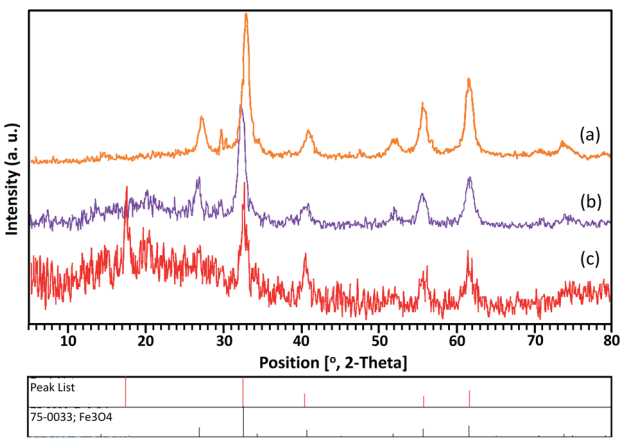

Fig. 2 The XRD patterns of (a) Fe_3O_4, (b) Fe_3O_4@SiO_2, and (c) Mag@Morph-AIL.

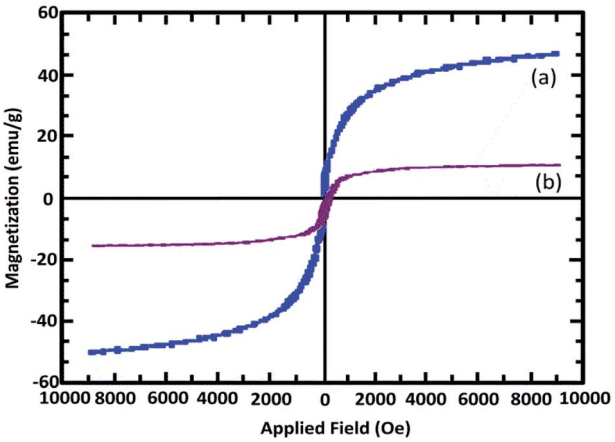

Fig. 3 Magnetization *versus* the applied field for (a) Fe_3O_4@SiO_2 and (b) Mag@Morph-AIL.

magnetic nanomaterial, with an average size of 69 nm, which shows close agreement with the value determined *via* SEM, while being larger than the value obtained *via* XRD analysis. Also, as seen in Fig. 5, the EDX spectrum of the synthesized Mag@Morph-AIL NP catalyst was obtained, in which the expected elemental composition (C, N, O, Si, S, and Fe) is shown clearly.

As shown in Fig. 6, the thermal behavior of the Mag@Morph-AIL nanocatalyst was studied. The TG profile exhibited two weight loss steps. An initial mass loss of 4% with an endothermic peak in the DTA curve is revealed in the temperature range of 100–150 °C. This can be related to the release of physically absorbed water on the surface of the nanomaterial. The second mass loss of 30% occurred in a wide temperature range of 420–500 °C, which overlapped with a broad endothermic DTA peak. This corresponds mainly to the thermal decomposition of the organic complex. The results of

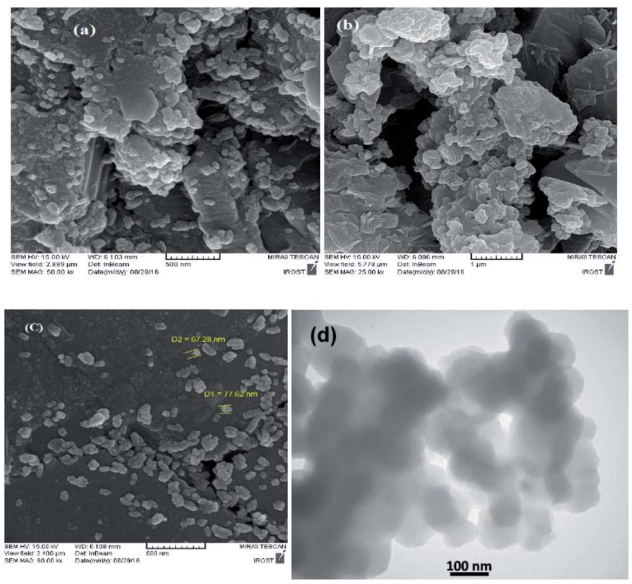

Fig. 4 SEM images of (a) Fe_3O_4, (b) Fe_3O_4@SiO_2, and (c) Mag@Morph-AIL, and (d) a TEM image of Mag@Morph-AIL.

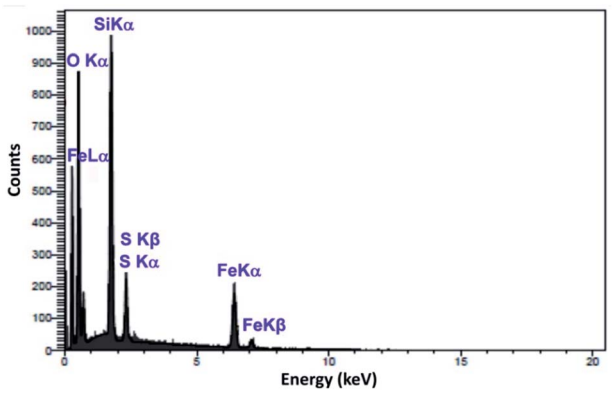

Fig. 5 The EDX spectrum of Mag@Morph-AIL.

thermal analysis revealed that the thermal decomposition of the organic moieties was completed at a temperature of 790 °C.

Thermogravimetric analysis can be used to estimate the amount of catalytically active species on the solid nanocomposite material. To calculate the amount of organic moieties (mmol g^{-1}), the solid catalyst weight-loss value of 26% w/w that can be attributed to organic functional groups was used in conjunction with the molecular weight of the organic moieties. According to these data, the amount of organic active species anchored on the surface of the solid catalyst is 1.070 mmol g^{-1}.

The amount of acid in the catalyst was quantitatively estimated *via* ion-exchange pH analysis.[47] For this purpose, 75 mg of solid catalyst was added to an aqueous solution of NaCl (1 M, 50 mL), and the resulting mixture was stirred for 3 days. The final mixture was titrated using 0.05 M NaOH solution. The amount of acid in the Mag@Morph-AIL catalyst was determined to be 1.862 mmol g^{-1}, which appears to be a good approximation because it is twice the amount of organic species estimated *via* TGA and each organic moiety has two acidic hydrogens.

Catalytic performance of the solid acidic ionic liquid for the Biginelli reaction

Mag@Morph-AIL, as an organic–inorganic hybrid nanomaterial, when used as a catalyst in the Biginelli reaction,

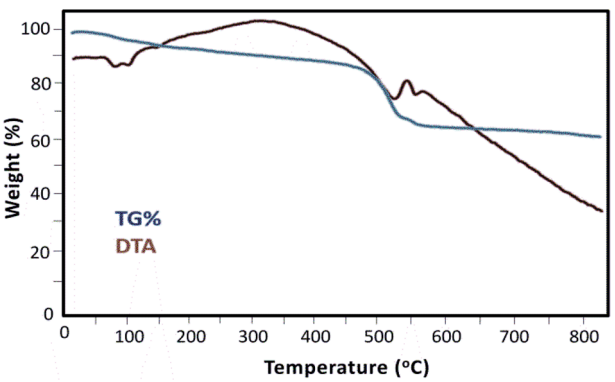

Fig. 6 TGA and DTA curves of Mag@Morph-AIL.

Scheme 2 The use of Mag@Morph-AIL in the Biginelli reaction.

showed significant advantages, such as biocompatibility, magnetic separability and recoverability, thermal stability, a high surface area, and a higher loading of active sites. Moreover, the introduction of sulfonic acid and organic groups onto the surface of Fe_3O_4@SiO_2 is interesting since the combination of both acidic and hydrophobic functionalities allows for the creation of a less-polar organic environment with relatively strong acidity, leading to a "quasi-homogeneous" catalyst for acid-catalyzed reactions. However, in many acid-catalyzed reactions using silica-based solid acids, the water produced as a by-product can be adsorbed on the surface of silanol, thus poisoning the surface, reducing the performance of the catalyst, and deactivating the active acidic sites of the catalyst.

To begin this study, the reaction conditions, such as the solvent, temperature, and the amount of catalyst, were optimized (Scheme 2). For this purpose, the reaction between benzaldehyde (1.0 mmol), ethyl acetoacetate (1.0 mmol), and urea (1.5 mmol) as substrates with the prepared nanocomposite material as a catalyst under reflux conditions was selected as the model reaction. At first, the optimum amount of catalyst was investigated in ethanol solvent (Table 1). It was found that the best results were obtained when the reaction was carried out in the presence of 0.06 g of catalyst (Table 1, entry 4).

In order to optimize the temperature of the reaction, the reaction was performed at different temperatures in the presence of 0.06 g of catalyst and with ethanol as the solvent. With reference to the results shown in Table 2, it was found that the best results were obtained when the reaction was carried out at 80 °C (Table 2, entry 3).

In an effort to obtain better yields and the most effective solvent, various solvents were used for the synthesis of 3,4-dihydropyrimidinones with a catalytic amount of Mag@Morph-AIL NPs in a simple reaction. With reference to the results in Table 3, polar and protic solvents increased the rate of reaction, and EtOH provided excellent yields and proved to be the solvent of choice.

In continuation of this research, as shown in Table 4, the corresponding products were obtained in excellent yields and with short reaction times under the optimum conditions. To ascertain the scope and limitations of this reaction, some aliphatic and aromatic aldehydes were refluxed with urea and ethyl acetoacetate in the presence of 0.06 g of Mag@Morph-AIL NPs with ethanol as the solvent at 80 °C. A best isolated yield of product of 93% was obtained within 58 min (Table 4). The desired 3,4-dihydropyrimidinone derivatives were synthesized and then characterized *via* spectroscopic methods.

Table 1 Optimization of the catalyst amount for the formation of 3,4-dihydropyrimidinones[a]

Entry	Catalyst amount (g)	Time (min)	Yield[b] (%)
1	0.01	150	70
2	0.02	100	75
3	0.04	80	92
4	0.06	60	92
5	0.08	60	92

[a] Reaction conditions: *p*-methyl benzaldehyde (1 mmol), ethyl acetoacetate (1 mmol), urea compound (1.5 mmol), and Mag@Morph-AIL catalyst were added to EtOH as the solvent (5 mL) at 80 °C. [b] Isolated yield.

Table 2 The effects of temperature on the synthesis of 3,4-dihydropyrimidinones[a]

Entry	Temperature (°C)	Time (min)	Yield[b] (%)
1	60	120	60
2	70	90	75
3	80	60	92
4	90	60	92

[a] Reaction conditions: *p*-methyl benzaldehyde (1 mmol), ethyl acetoacetate (1 mmol), urea compound (1.5 mmol) and Mag@Morph-AIL catalyst (0.06 g) were refluxed in EtOH (5 mL). [b] Isolated yield.

Reusability of the Mag@Morph-AIL nanocatalyst

The Mag@Morph-AIL nanocatalyst is recoverable without a considerable loss of catalytic activity. After the completion of the reaction, 5 mL of ethanol was added to the reaction mixture and the nanocatalyst was recycled using an external magnetic field and washed with acetone to remove residual product or other organic material. The nanocatalyst was reused for a new Biginelli reaction between *p*-methyl benzaldehyde, ethyl acetoacetate, and urea under similar reaction conditions. As shown in Fig. 7, the NPs could be reused for up to eight cycles with an insignificant loss of catalytic activity, providing the product in high yields.

Table 3 The effects of the solvent on the synthesis of 3,4-dihydropyrimidinones[a]

Entry	Catalyst amount (g)	Time (min)	Yield[b] (%)
1	THF	150	50
2	CH_3CN	130	44
3	EtOH	60	92
4	DMSO	120	35

[a] Reaction conditions: *p*-methyl benzaldehyde (1 mmol), ethyl acetoacetate (1 mmol), urea compound (1.5 mmol), and Mag@Morph-AIL catalyst (0.06 g) were refluxed in the selected solvent (5 mL) at 80 °C. [b] Isolated yields.

Table 4 The synthesis of 3,4-dihydropyrimidinones using Mag@Morph-AIL[a]

Entry	Name	Product[b]	Time (min)	Yield[c] (%)	MP[d] (°C)
1	**4a**	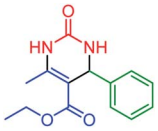	64	86	204–206 (ref. 47)
2	**4b**	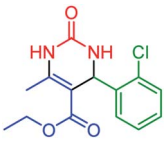	65	88	252–253 (ref. 48)
3	**4c**	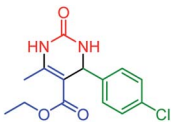	60	87	206–208 (ref. 49)
4	**4d**	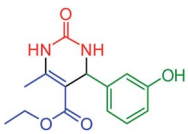	70	85	167–170 (ref. 49)
5	**4e**	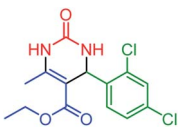	60	89	251–254 (ref. 49)
6	**4f**	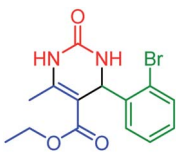	65	86	185–188 (ref. 44)
7	**4g**	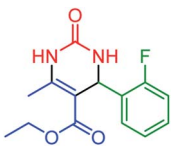	70	88	224–225 (ref. 52)
8	**4h**	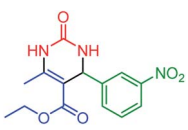	60	90	123–126 (ref. 47)
9	**4i**	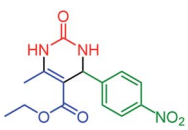	58	93	205–208 (ref. 51)
10	**4j**	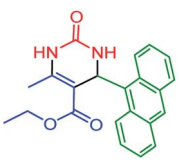	70	89	283–285 (ref. 53)

Table 4 (*Contd.*)

Entry	Name	Product[b]	Time (min)	Yield[c] (%)	MP[d] (°C)
11	**4k**	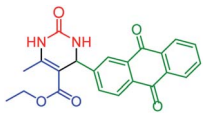	66	91	272–275 (ref. 52)
12	**4l**	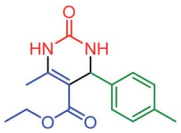	60	92	206–207 (ref. 49)
13	**4m**	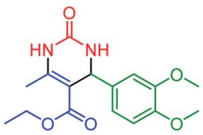	75	85	176–179 (ref. 49)
14	**4n**	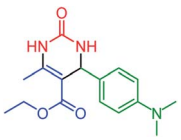	75	87	258–261 (ref. 50)
15	**4o**	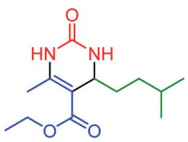	80	80	169–173 (ref. 44)

[a] Reaction conditions: benzaldehyde (1 mmol), ethyl acetoacetate (1 mmol), urea compound (1.5 mmol) and Mag@Morph-AIL catalyst (0.06 g) were refluxed in EtOH as the solvent (5 mL). [b] All products were characterized based on their spectroscopic data (FT-IR and 1H-NMR). [c] Isolated yield. [d] Literature reference.

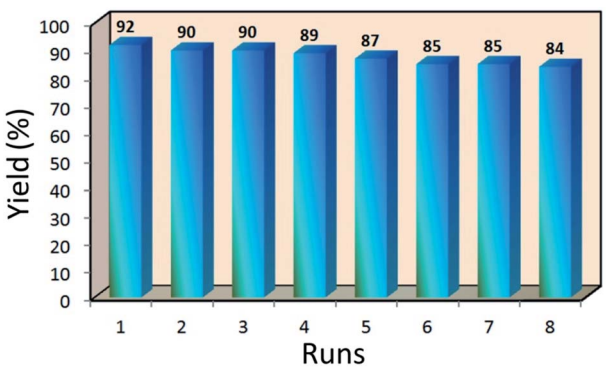

Fig. 7 Recyclability study of Mag@Morph-AIL.

Conclusions

In this report, we have developed a straightforward and efficient method for the synthesis of 3,4-dihydropyrimidinones using a Mag@Morph-AIL nanocomposite material as a new metal-free catalyst. The novel magnetic recoverable nanocatalyst was characterized using FT-IR, SEM, EDX, XRD, VSM, and BET techniques. The catalyst showed excellent efficiency and could convert >92% of the substrates to the target molecules within 60 min at 78 °C. The catalyst was recovered using an external magnet from the reaction mixture and could be recycled for at least 8 runs without a major decrease in catalytic activity. The method offers several advantages, including clean reaction profiles, good availability, high yields, short reaction times, simple experimental procedures, catalyst reusability, and low catalyst loading.

Conflicts of interest

There are no conflicts to declare.

Acknowledgements

The authors are grateful to the University of Kashan for supporting this work (grant no. 159148).

Notes and references

1 T. Peters, H. Lindenmaier, W. Haefeli, J. Weiss and N. S. Arch, *Pharmacology*, 2006, **372**, 291–299.
2 J. C. Cochran, J. E. Gatial, T. M. Kapoor and S. P. Gilbert, *J. Biol. Chem.*, 2005, **280**, 12658–12667.
3 S. Tcherniuk, R. van Lis, F. Kozielski and D. A. Skoufias, *Biochem. Pharmacol.*, 2010, **79**, 864–872.
4 K. De, S. Chandra, B. Sarkar, S. Ganguly and M. Misra, *J. Radioanal. Nucl. Chem.*, 2010, **283**, 621–628.
5 I. M. T. C. Crevel, M. C. Alonso and R. A. Cross, *Curr. Biol.*, 2004, **14**, R411–R412.
6 S. H. Choi and D. McCollum, *Curr. Biol.*, 2012, **22**, 225–230.
7 J. C. Cochran and S. P. Gilbert, *Biochem*, 2005, **44**, 16633–16648.
8 L. Duan, T.-Q. Wang, W. Bian, W. Liu, Y. Sun and B.-S. Yang, *Spectrochim. Acta, Part A*, 2015, **137**, 1086–1091.
9 S. DeBonis, J. P. Simorre, I. Crevel, L. Lebeau, D. A. Skoufias, A. Blangy, C. Ebel, P. Gans, R. Cross, D. D. Hackney, R. H. Wade and F. Kozielski, *Biochemistry*, 2003, **42**, 338–349.
10 K. Drosopoulos, C. Tang, W. C. H. Chao and S. Linardopoulos, *Nat. Commun.*, 2014, **5**, 3686.
11 C. J. Funk, A. S. Davis, J. A. Hopkins and K. M. Middleton, *Anal. Biochem.*, 2004, **329**, 68–76.
12 R. V. Chikhale, R. P. Bhole, P. B. Khedekar and K. P. Bhusari, *Eur. J. Med. Chem.*, 2009, **44**, 3645–3653.
13 C. O. Kappe, *Eur. J. Med. Chem.*, 2000, **35**, 1043–1052.
14 L. H. S. Matos, F. T. Masson, L. A. Simeoni and M. Homem-de-Mello, *Eur. J. Med. Chem.*, 2018, **143**, 1779–1789.
15 P. Biginelli, *Gazz. Chim. Ital.*, 1883, **23**, 360–413.
16 (*a*) S. S. Panda, P. Khanna and L. Khanna, *Curr. Org. Chem.*, 2012, **16**, 507–520; (*b*) M. H. Majid, S. Asadi and B. M. Boshra, *Mol. Diversity*, 2013, **17**, 389–407; (*c*) C. de-Graaff, E. Ruijter and R. V. A. Orru, *Chem. Soc. Rev.*, 2012, **41**, 3969–4009.
17 A. S. Paraskar, G. K. Dewkar and A. Sudalai, *Tetrahedron Lett.*, 2003, **44**, 3305–3308.
18 K. A. Kumar, M. Kasthuraiah, C. S. Reddy and C. D. Reddy, *Tetrahedron Lett.*, 2001, **42**, 7873–7875.
19 M. Gohain, D. Prajapati and J. S. Sandhu, *Synlett*, 2004, **2**, 0235–0238.
20 C. Simon, T. Constantieux and J. Rodriguez, *Eur. J. Org. Chem.*, 2004, 4957–4980.
21 J. S. Yadav, B. V. S. Reddy, P. Sridhar, J. S. S. Reddy, K. Nagaiah, N. Lingaiah and P. S. Saiprasad, *Eur. J. Org. Chem.*, 2004, 552–557.
22 C. O. Kappe and S. F. Falsone, *Synlett*, 1998, 718–720.
23 (*a*) S. Xue, Y.-C. Shen, Y.-L. Li, X.-M. Shen and Q.-X. Guo, *Chin. J. Chem.*, 2002, **20**, 385–389; (*b*) J. Lu and H. Ma, *Synlett*, 2000, 63–64.
24 (*a*) V. R. Choudhary, V. H. Tillu, V. S. Narkhede, H. B. Borate and R. D. Wakharkar, *Catal. Commun.*, 2003, **4**, 449–453; (*b*) S. E. Hankari, B. Motos-Pérez, P. Hesemann, A. Bouhaouss and J. J. E. Moreau, *Chem. Commun.*, 2011, **47**, 6704–6706.
25 J. Safari and S. G. Ravandi, *J. Mol. Catal. A: Chem.*, 2013, **373**, 72–77.
26 J. Safaei-Ghomi, R. Teymuri and A. Ziarati, *Monatsh. Chem.*, 2013, **144**, 1865–1870.
27 H. R. Memarain and M. Ranjbar, *J. Mol. Catal. A: Chem.*, 2012, **356**, 46.
28 J. Javidi, M. Esmaeilpour and F. N. Dodeji, *RSC Adv.*, 2015, **5**, 308–315.
29 B. K. Banik, A. T. Reddy, A. Datta and C. Mukhopadhyay, *Tetrahedron Lett.*, 2007, **48**, 7392–7394.
30 J. Safari and S. Gandomi-Ravandi, *New J. Chem.*, 2014, **38**, 3514–3521.
31 J. T. Li, J. F. Han, J. H. Yang and T. S. Li, *Ultrason. Sonochem.*, 2003, **10**, 119–122.
32 J. Peng and Y. Deng, *Tetrahedron Lett.*, 2001, **42**, 5917–5919.
33 A. Zhu, Q. Li, L. Li and J. Wang, *Catal. Lett.*, 2013, **143**, 463–468.
34 M. Rahman, A. Sarkar, M. Ghosh, A. Majee and A. Hajra, *Tetrahedron Lett.*, 2014, **55**, 235–239.
35 S. Verma, S. L. Jain and B. Sain, *Tetrahedron Lett.*, 2010, **51**, 6897–6900.
36 M. Faraji, Y. Yamini and M. Rezaee, *J. Iran. Chem. Soc.*, 2010, **7**, 1–37.
37 L. M. Rossi, N. J. S. Costa, F. P. Silva and R. V. Goncalves, *Nanotechnol. Rev.*, 2013, **2**, 597–614.
38 S. J. Wang, Z. Y. Wang and Z. G. Zha, *Dalton Trans.*, 2009, **43**, 9363–9373.
39 R. B. N. Baig and R. S. Varma, *Chem. Commun.*, 2013, **49**, 752–770.
40 Q. He, W. Wu and C. Jiang, *Nanoscale Res. Lett.*, 2008, **3**, 397–415.
41 R. Y. Hong, B. Feng, G. Liu, S. Wang, H. Z. Li, J. M. Ding, Y. Zheng and D. G. Wei, *J. Alloys Compd.*, 2009, **476**, 612–618.
42 M. H. Valkenberg, C. de Castro and W. F. Holderich, *Green Chem.*, 2002, **4**, 88–93.
43 S. A. Galema, *Chem. Soc. Rev.*, 1907, **26**, 233–238.
44 M. Bagherzadeh, M. Haghdoost, F. Matlobi-Moghaddam, B. Koushki-Foroushani, S. Sarazdi and E. Payab, *J. Coord. Chem.*, 2013, **66**, 3025–3036.
45 A. Shaabani, A. Bazgir and F. Teimouri, *Tetrahedron Lett.*, 2003, **44**, 857–859.
46 D. Azarifar, O. Badalkhani and Y. Abbasi, *J. Sulfur Chem.*, 2016, **37**, 1–18.
47 (*a*) Q. Zhang, H. Su, J. Luo and Y. Wei, *Green Chem.*, 2012, **14**, 201–208; (*b*) E. G. Derouane, J. C. Védrine, R. R. Pinto, P. M. Borges, L. Costa, M. A. N. D. A. Lemos, F. Lemos and F. R. Ribeiro, *Catal. Rev.: Sci. Eng.*, 2013, **55**, 454–515.
48 C. O. Kappe, *Tetrahedron*, 1993, **49**, 6937–6963.
49 A. Mobinikhaledi and M. A. Bodaghi-Fard, *Acta Chim. Slov.*, 2010, **57**, 931–935.
50 Y. Ma, C. Qian, L. Wang and M. Yang, *J. Org. Chem.*, 2000, **65**, 3864–3868.
51 J. Lu and Y. Bai, *Synthesis*, 2002, 0466–0470.
52 G. Aridoss and Y. T. Jeong, *Bull. Korean Chem. Soc.*, 2010, **31**, 863–868.
53 K. Konkala, N. M. Sabbavarapu, R. Katla, N. Y. V. Durga, V. K. Reddy, B. L. A. Prabhavathi-Devi and R. B. N. Prasad, *Tetrahedron Lett.*, 2012, **53**, 1968–1973.